Entanglement transition and heterogeneity in long-range quadratic Lindbladians

Alejandro Cros Carrillo de Albornoz, Dominic C. Rose, and Arijeet Pal
Department of Physics and Astronomy, University College London, Gower Street, London WC1E 6BT, United Kingdom

(Received 28 March 2023; revised 16 May 2024; accepted 16 May 2024; published 11 June 2024)

The generation of entanglement in mixed states is relevant to quantum systems coupled to an environment. The dissipative and mixing properties of the environment are unavoidable in physical platforms for quantum simulation and information processing, where entanglement can be a vital resource. In this work, we explore entanglement and heterogeneity in random Lindbladian dynamics describing open quantum systems. We propose a model of a one-dimensional chain of noninteracting, spinless fermions coupled to a local ensemble of baths. The jump operator mediating the interaction with the bath linked to each site has a power-law tail with an exponent p. We show that the system undergoes volume-to-area law entanglement phase transition in the mixed steady state by tuning p which remains stable in the presence of coherent hopping. Unlike the entanglement transition in the pure-state quantum trajectories of open systems, this transition is exhibited by the averaged steady-state density matrix of the Lindbladian. The steady state in the area-law phase is characterized by a spatial heterogeneity in local population imbalance, while the jump operators exhibit a constant participation ratio of the sites they affect. Our work provides a theoretical description of an entanglement transition realized in long-ranged open quantum systems and provides an avenue to stabilize quantum correlations in mixed states.

DOI: 10.1103/PhysRevB.109.214204

I. INTRODUCTION

Interactions of a quantum system with an environment can destroy quantum correlations. The environment disrupts the fragile nature of a quantum superposition which encodes entanglement and quantum information [1–5]. The stability of quantum entanglement in the presence of dissipation can prove to be vital for discovery of new quantum phenomena in the laboratory and developing technologies for quantum sensing and information processing [6–8]. A precise understanding of the evolution of long-range quantum correlations in the presence of dissipation provides a picture of thermalization and formation of states which deviate from the thermal ensemble going beyond isolated systems [9,10]. In this context, the temporal and spatial properties of the environment, which control the dissipative processes, play an important role in the relaxation dynamics and the formation of novel steady states [11–15].

Open quantum systems (OQSs) can host steady states which are manifestly out of equilibrium and protect coherence from environmental noise, such as decoherence-free subspaces [16–18] and noiseless subsystems [19,20], among other nonequilibrium phenomena [21–25]. The long-time dynamics leading to stationarity may present complex metastable behavior [26–29], while periodic driving can enable time-crystalline phenomena [30–37]. Quantum trajectories of OQSs, providing stochastic realizations of the systems pure-state evolution, can exhibit nontrivial statistics that cannot be detected in either the averaged time evolution of the density matrix or its steady state [38–47]. In particular, recent work demonstrating entanglement transitions in quantum trajectory ensembles has spurred interest for quantum information processing [48–50]. Altogether, the preservation of coherence in nonequilibrium OQSs suggests the possibility for new quantum behavior to survive in the presence of dissipation.

Quadratic Lindbladians have emerged as a test bed for studying various concepts in OQSs [51–61], due to simplifications enabled by their noninteracting nature. Here we propose and investigate the properties of a quadratic fermionic Lindbladian model which undergoes a volume-to-area law entanglement phase transition induced by coupling to a heterogeneous bath. The local degrees of freedom couple randomly to baths, similarly to recent work on random Lindbladians [62–72], with correlations decaying as a power law in space. The baths are modeled using a Lindbladian formalism for OQSs where the jump operators influence distant sites, realizable in the collective dissipation of atomic arrays [73–80]. The locality of the jump operators representing the bath-mediated interaction is a tunable parameter, driving a phase transition between volume and area law entangled steady states, the strength of their influence decaying as a power law in separation between sites in the area-law phase. The steady-state properties closely relate to the single-particle localization transition of power-law random banded matrices (PRBMs) for purely unitary dynamics, with the correlation matrix exhibiting analogous statistical properties [81–88]. Furthermore, we studied the effect of coherent hopping on the system's dynamics and steady state, finding that the phenomena observed—

including the transition—are largely independent of such perturbations.

II. MODEL

We consider a one-dimensional spinless fermionic system modeled by a quadratic Lindblad equation $\frac{d}{dt}\rho(t) = \mathcal{L}(\rho)$, with Lindblad operator

$$\mathcal{L}(\rho) = -i[H, \rho(t)] + \sum_{jk} \Gamma_{jk}\left(c_k^\dagger \rho(t) c_j - \frac{1}{2}\{c_j c_k^\dagger, \rho(t)\}\right) + \sum_{jk} B_{jk}\left(c_j \rho(t) c_k^\dagger - \frac{1}{2}\{c_k^\dagger c_j, \rho(t)\}\right), \quad (1)$$

in terms of fermionic creation operators $c_j^\dagger$ at sites j, where the Hamiltonian $H = \sum_{n,m} h_{nm} c_n^\dagger c_m$ conserves particle number governed by Hermitian matrix h. Specifically, we will consider coherent hopping, corresponding to $h_{nm} = \lambda$ if $m = n \pm 1$ and 0 otherwise.

The dissipative bath interactions include particle creation and annihilation governed by positive-semidefinite matrices Γ and $B = I - \Gamma$, respectively. The action of the bath on the system can be more clearly seen in the diagonal form of the dissipator,

$$\mathcal{L}(\rho) = -i[H, \rho(t)] + \sum_m \gamma_m\left(d_m^\dagger \rho(t) d_m - \frac{1}{2}\{d_m d_m^\dagger, \rho(t)\}\right) + \sum_m (1-\gamma_m)\left(d_m \rho(t) d_m^\dagger - \frac{1}{2}\{d_m^\dagger d_m, \rho(t)\}\right), \quad (2)$$

where γ_m are eigenvalues of Γ and $d_m = \sum_i \langle i|g_m\rangle c_i$ are jump operators describing the action of the bath, given by the corresponding eigenvectors of Γ, $\Gamma|g_m\rangle = \gamma_m|g_m\rangle$.

We wish to model a bath which acts on the system heterogeneously, through changes that can be tuned to have different degrees of locality. To achieve this while maintaining Hermiticity and positivity of Γ we take $\Gamma \propto X^\dagger X$ for a random matrix X. The elements of X are chosen as

$$X_{jk} = \frac{x_{jk}}{(|j-k|+1)^p}, \quad (3)$$

where x_{jk} is chosen from the complex Gaussian distribution $\mathcal{CN}(0, 1)$, and p controls the decay of matrix elements with distance from the diagonal, analogous to PRBMs and Wishart matrices. As we will see, the value of p directly influences how localized the eigenvectors of Γ are, and thus how localized the jump operators are, leading to the model sketched in Fig. 1(a). Each site can be imagined to have an associated bath, interacting with the system with distinct rates representing differing energies of the modes or different temperatures of the baths, encoded in the eigenvalues of Γ. Bath interactions are mediated via the jump operators d_m, adding or removing particles from modes focused on the associated site and decaying away from that site as a power law with an exponent determined by p, as demonstrated in Fig. 11 in Appendix E 3. Such long-range jump operators with a power-law spatial profile can be realized with cold atoms in optical cavities using tunable Raman sidebands for the driving field as discussed in [75].

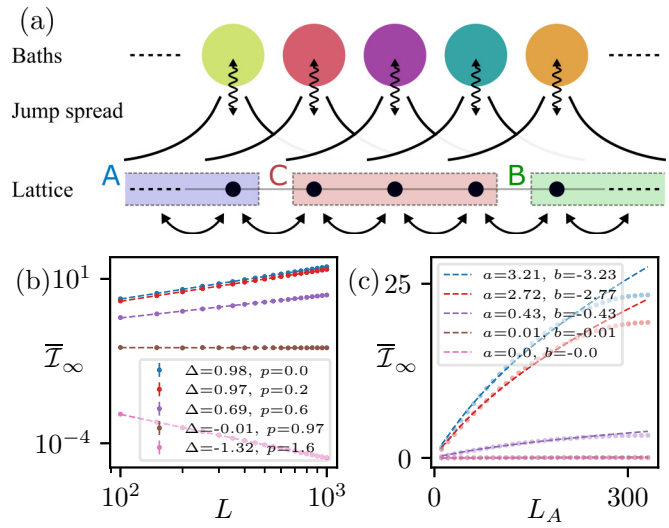

FIG. 1. (a) Schematic of the model: The spatial power-law profile of each jump operator for the heterogeneous baths shows the coupling to a system of spinless fermions hopping in a 1D lattice. We consider the mutual information between fermions in regions A and B ($\mathcal{I}$). (b) Disorder-averaged mutual information between A and B in the steady state ($\overline{\mathcal{I}}_\infty$) as a function of system size L, with $L_A = L_B = L_C = L/3$. For each value of p (shown in the legend) the curves are fitted to the form $\ln(\overline{\mathcal{I}}_\infty) = \Delta \ln(L) + c$. The fitting parameter Δ is shown in the legend. (c) $\overline{\mathcal{I}}_\infty$ between A and B in the steady state as a function of subsystem size L_A with total system size $L = 10^3$. L_C is fixed at $L/3$. Curves were fitted according to $\overline{\mathcal{I}}_\infty = a(L_A)^c + b\log(L_A)$. Note $c \approx 1/2$ for all p. For both (b), (c): Curves are color coded to a given p according to the legend in panel (b). Error bars are not visible. Details on disorder realizations are included in Appendix H 1.

Note, for the dissipative evolution to be valid, the maximum eigenvalue of Γ must be less than 1, so we scale the product by twice its maximum eigenvalue, denoted $\lambda_{\max}$, i.e., $\Gamma = X^\dagger X/2\lambda_{\max}$. Alternatively, one may use the Kac normalization in Ref. [36]. The overall scaling does not affect the local properties or steady state, which will be the focus of our work.

III. GAUSSIANITY AND PURE DISSIPATION SOLUTION

The quadratic structure of the Lindbladian results in a closed equation for the time evolution of the two-point correlation matrix $\Omega_{jk} = \mathrm{Tr}(\rho c_j^\dagger c_k)$ [55], giving

$$\frac{d\Omega}{dt} = i[h^T, \Omega] + \frac{1}{2}(\{\Gamma, \mathbb{I} - \Omega\} - \{\mathbb{I} - \Gamma, \Omega\}). \quad (4)$$

The first term corresponds to the coherent Hamiltonian evolution, the second term corresponds to bath interactions which create fermions, while the third term removes them. This implies that beginning from a Gaussian state leaves the state Gaussian at all times, and that the steady state will be Gaussian. We thus restrict our attention to Gaussian states described by this equation.

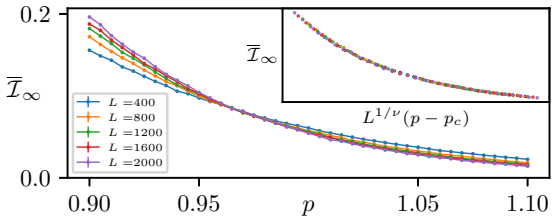

FIG. 2. Mutual information between A and B as a function of p, with $L_A = L_B = L_C = L/3$, for various L shown, averaged over disorder. Inset shows a finite-size scaling collapse with $p_c = 0.98 \pm 0.01$ and $\nu = 6.3 \pm 0.7$. Error bars are not visible. Details on disorder realizations and fitting procedure are included in Appendix H.

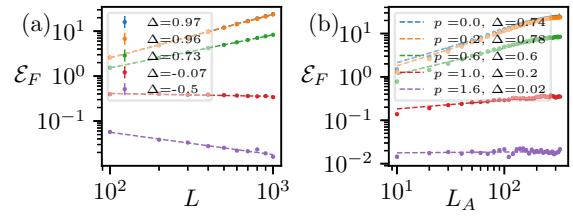

FIG. 3. (a) Disorder-averaged fermionic negativity ($\mathcal{E}_F$) between A and B (cf. Fig. 1) in the steady state as a function of system size L, with $L_A = L_B = L_C = L/3$. (b) Steady state $\mathcal{E}_F$ between A and B as a function of subsystem size L_A with $L_C = L/3$ fixed at $L = 10^3$. For each value of p the curves are fitted to $\ln[f(x)] = \Delta \ln(x) + c$. The corresponding Δ is shown in the legend. Details on disorder realizations are included in Appendix H 1.

The steady state and time evolution can be solved exactly both with and without a Hamiltonian. We begin with the Hamiltonian-free case ($\lambda = 0$), finding

$$\Omega(t) = \Gamma(1 - e^{-t}) + \Omega(0)e^{-t}. \tag{5}$$

The steady-state correlation matrix is unique, $\Omega(0) = \Gamma$ in this case. The parameter p allows us to tune between two limits. When p is large, Γ is short-ranged and almost diagonal; thus the steady state is approximately unentangled. In contrast, $p = 0$ implies Γ is infinite-ranged and random, and one would expect the steady state to be entangled and obey a volume law [89,90]. In this work, we study what happens between the two limits as p is varied.

IV. MUTUAL INFORMATION

We first consider the correlations in the steady state as we vary p using the mutual information $\mathcal{I}$ (denoted by $\mathcal{I}_\infty$, with disorder average $\overline{\mathcal{I}}_\infty$), defined between subsystems A and B as

$$\mathcal{I}_{A|B}(\rho) = S_A(\rho) + S_B(\rho) - S_{A\cup B}(\rho), \tag{6}$$

where $S_X(\rho)$ is the von Neumann entropy of ρ in subsystem X, which may be rewritten in terms of the subsystem correlation matrix Ω_X of ρ as $S_X(\rho) = -\mathrm{Tr}[\Omega_X \ln(\Omega_X) + (1 - \Omega_X)\ln(1 - \Omega_X)]$ [91,92].

We choose subsystems A and B separated by an intervening region C of length $L_C = L/3$ to remove boundary correlation terms, cf. Fig. 1(a), and consider two cases: varying overall system size L with $L_A = L_B = L/3$, and varying subsystem size L_A for a fixed L (see Appendix F for the case with boundaries). In the first case in Fig. 1(b) we observe that for small p, $\overline{\mathcal{I}}_\infty$ scales as a volume law in L, as expected; for large p the lack of boundary terms causes $\overline{\mathcal{I}}_\infty$ to decay toward zero with increasing L. At intermediate values of p we observe power-law behavior, with exponent Δ decreasing as p increases until a critical point $p = p_c$ at which $\overline{\mathcal{I}}_\infty$ is approximately constant as a function of L. As p increases further, Δ becomes negative. This p dependence of Δ is suggestive of a transition between area and volume law entanglement phases.

In Fig. 2 we perform a scaling collapse assuming a continuous transition finding a critical point at $p_c = 0.98 \pm 0.01$ with a correlation length critical exponent of $\nu = 6.3 \pm 0.7$. The critical point is close to the localization transition for PRBMs of $p_c \sim 1$, suggesting that the transition is driven by the localization of the effective jump operators d_m. Nevertheless, our analysis of the correlations in the steady state differs from the existing studies of entanglement in eigenstates of PRBM models. However, the volume-law phase close to the transition exhibits a sub-volume-law scaling in $\mathcal{I}$ in analogy with the eigenstate entanglement transition of PRBM models [93–95]. We note that this scaling is possibly due to classical correlations as the scaling of fermionic negativity, a direct measure of quantum correlations, does not show this effect (see next section). Interestingly, the critical exponent ν is comparable in size to the exponents for measurement-induced transitions for quantum trajectories studied in long-range Clifford circuits and free-fermion Hamiltonians [96–99].

In Fig. 1(c) we see that with L_C fixed at $L/3$, $\overline{\mathcal{I}}_\infty$ is independent of subsystem size L_A in the area-law phase at large p. In contrast, the volume-law phase at small p exhibits a subextensive scaling of $\overline{\mathcal{I}}_\infty$, differing from the linear dependence seen in volume-law entangled pure states. Regardless, our results suggest that even for $p \sim 0$, when $\overline{\mathcal{I}}_\infty$ scales as a volume law with system size, the scaling with L_A is subextensive. A possible explanation could be that the steady states, although delocalized, are only weakly entangled locally. This would be analogous to delocalized, nonergodic states discussed in the context of Anderson localization on Bethe lattices [100,101].

V. FERMIONIC NEGATIVITY

Since mutual information contains contributions from classical correlations, to capture quantum correlations we consider the *fermionic negativity* $\mathcal{E}_F$. A version of entanglement negativity [102,103] that is tailored to Gaussian fermionic systems [104,105], this captures entanglement even in mixed states, and is expressed as

$$\mathcal{E}_F = \sum_j \ln[\sqrt{\mu_j} + \sqrt{1 - \mu_j}] + \sum_j \frac{1}{2} \ln[(\lambda_j)^2 + (1 - \lambda_j)^2], \tag{7}$$

where μ_j and λ_j are eigenvalues of two algebraic expressions of the two-point correlator Ω [105]. In Fig. 3 we show the variation of $\mathcal{E}_F$ with system size (L) and subsystem size (L_A). We note that while $\mathcal{I}(L_A)$ (cf. Fig. 1) suffers from finite-size effects which become apparent in a log-log scale—all curves scale in the same manner albeit the magnitude of $\mathcal{I}$ in the area law is $\mathcal{O}(10^{-7})$—these finite-size effects vanish in $\mathcal{E}_F(L_A)$,

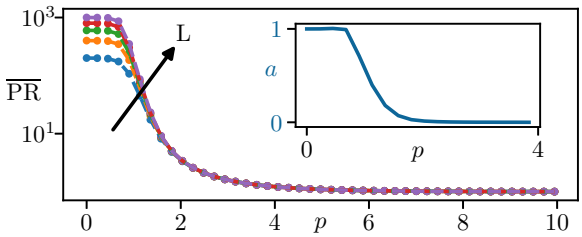

FIG. 4. The disorder-averaged participation ratio $\overline{\mathrm{PR}}$ against p for sizes $L = [400, 800, 1200, 1600, 2000]$, increasing along the arrow. Inset: Power a as a function of p found when fitting $\overline{\mathrm{PR}}(L, p) = L^{a(p)}/c(p)$ to $\overline{\mathrm{PR}}(L)$ curves. Data for c are shown in Appendix D.

suggesting they are the result of the mixed nature of the steady state.

VI. BATH STRUCTURE

The entanglement transition occurs in parallel with structural changes of the bath, observable through the eigenvectors of Γ in the Lindblad equation, which determines its jump operators as $d_m = \sum_i \langle i|g_m\rangle c_i$, where $\Gamma\,|g_m\rangle = \gamma_m\,|g_m\rangle$. We thus consider the participation ratio (PR) of the eigenstates g_m of Γ, a measure of their locality, defined as $\mathrm{PR}(g) = \frac{1}{\sum_m |g_m|^4}$.

In Fig. 4 we show $\overline{\mathrm{PR}}$, the PR averaged over eigenvectors of Γ from multiple disorder realizations. Varying p leads to a transition: from delocalized vectors where the $\overline{\mathrm{PR}}$ grows linearly with L, with $d_n \sim \sum_n c_n$ such that the bath correlates distant sites, to localized vectors where it becomes small and constant, with the bath jump operator $d_n \sim c_n$ acting on a single site. However, rather than a sharp transition, we see a gradual reduction in the constant value that the PR achieves as p increases, approximately reaching its lower bound of 1 at large p. To characterize this, in the inset of Fig. 4 we show the p dependence of a power-law fit of $\overline{\mathrm{PR}}(L)$. Increasing p from the suspected critical point around $p = 1$, we see a decay from the expected exponent of 1 in the volume-law phase down to 0 in the area-law phase.

A possible explanation for the slow decay of the PR may be found in the localization behavior of the eigenstates. In Appendix E 3 we observe that the eigenstates of Γ exhibit a power-law decay away from some central site, similar to prior studies of PRBM models [106], in contrast with the exponential decay common in short-range models exhibiting localization. Relatedly, in Appendix C we also report observing multifractality in the eigenstates, a common phenomenon in PRBM models [107–109].

VII. STATIONARY-STATE HETEROGENEITY

We now investigate the impact of the *spatial* structure of the bath on the system's steady state. As portrayed in Fig. 4, the action of the bath is localized to a single site in the large-p limit due to Γ becoming increasingly diagonal in the position basis, causing a heterogeneous bath structure. In contrast, for p close to 0, the action of the bath is highly nonlocal, with each site affected by multiple jump operators which fluctuate weakly across different sites. This results in an effective homogeneity of the bath action when averaged over the jump operators, which can be viewed as a consequence of a central limit theorem. We expect this heterogeneous-vs-homogeneous behavior to be reflected in the properties of the steady state, as we will now show.

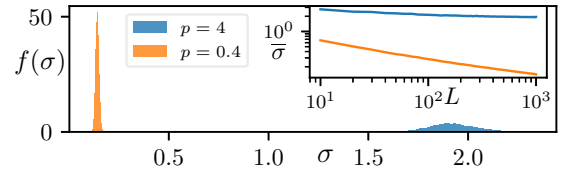

FIG. 5. Distribution of the standard deviation of the bias $\tilde{n}$ calculated for each realization using the central $L/5$ sites in the bulk in the area (blue, $p = 4$)) and volume law (orange, $p = 0.4$) phases for system size $L = 10^3$. Inset: Average standard deviation as a function of L; error bars are not visible.

To illustrate such behavior in our system, we calculate the variability of single-site density matrices in the steady state, which are diagonal due to Gaussianity. We write $\rho_s = Z_{\tilde{n}}\,|o\rangle\,\langle o| + (1 - Z_{\tilde{n}})\,|u\rangle\,\langle u|$ with $Z_{\tilde{n}} = e^{-\tilde{n}}/(1 + e^{-\tilde{n}})$, where $|o\rangle$ and $|u\rangle$ correspond to the single site s being occupied and unoccupied, and $\tilde{n}$ is the bias of that site toward being unoccupied.

We study the distribution of $\tilde{n}$ for $p = 0.4$ and $p = 4$. Figure 5 shows the standard deviation σ distribution of $\tilde{n}$ from the sites within the middle $1/5$ of the chain calculated in multiple disorder realizations. Note $\tilde{n}$ is mostly positive due to the spectra of Γ being in the interval $[0, 1/2]$, causing a lower rate of particle creation than annihilation, biasing sites to be unoccupied. In the volume-law phase ($p = 0.4$), the distribution is sharp and well defined at small values whereas the area law phase ($p = 4$) exhibits a distribution that is broad at much larger values: a signature of a heterogeneous system. The inset of Fig. 5 shows the scaling of the average standard deviation of $\tilde{n}$ against L, which is weak in the area-law phase but quickly sharpens in the volume-law phase as L increases, implying a homogeneous steady state in the thermodynamic limit. Reduced fluctuations in the volume-law phase are consistent with the increased mixing allowed by longer-range jump operators, as particles are distributed across the system, causing each site to equilibrate with each other.

VIII. EFFECT OF COHERENT HOPPING

To study the influence of a coherent dynamics on the steady state and dynamics, we introduce a nearest neighbor hopping Hamiltonian, $\lambda \neq 0$. Solving Eq. (4) in the eigenbasis of a Hamiltonian, we arrive at

$$\tilde{\Omega}(t)_{nm} = \left(\tilde{\Omega}(0)_{nm} - \frac{i\tilde{\Gamma}_{nm}}{\Delta E_{nm}}\right) e^{i\Delta E_{nm} t} + \frac{i\tilde{\Gamma}_{nm}}{\Delta E_{nm}}, \qquad (8)$$

where E_n are the eigenvalues of h, $\Delta E_{nm} \doteq E_n - E_m + i$, and $\widetilde{O}_{nm}$ denotes the matrix elements of O in h's basis. We note Eq. (8) holds for any h.

A unit relaxation timescale originates from $h = 0$. Here, creation and annihilation operators for the fermionic eigenmodes each contribute $-1/2$ to the eigenvalue. Since this equation describes the evolution of quadratic Gaussian operators, these eigenmodes appear in pairs whose eigenvalues

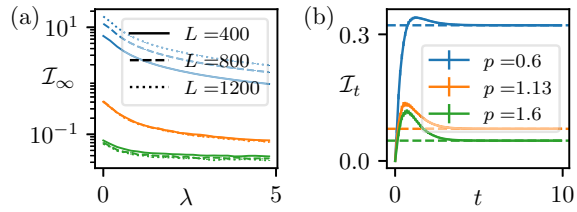

FIG. 6. (a) Dynamics of the bipartite mutual information $\overline{\mathcal{I}}_t$ between A and B where $L_A = L_B = L/2$ and $L_C = 0$, of an initially uncorrelated state, i.e., $\Omega(0) = \mathrm{diag}\{a_1, \ldots, a_L\}$, for random real $\{a_n\}$ with system size $L = 100$ and $\lambda = 5$. Dashed lines here denote their associated $\overline{\mathcal{I}}_\infty$. (b) Nonequilibrium steady state bipartite mutual information $\overline{\mathcal{I}}_\infty$ against hopping strength λ for different dissipation and system sizes. All curves were averaged over disorder realizations, and error bars are not visible.

sum to -1. For details see Appendix B. This implies that the timescale is independent of system size, p, and details of the dissipation.

In short, we see that turning on hopping does not affect the qualitative behavior of the model. Fig. 6(a) shows $\overline{\mathcal{I}}_\infty$ between A and B in the steady state, $L_A = L_B = L/2$ and $L_C = 0$: the L dependence of the two phases is unchanged, with the same critical point, although the $\overline{\mathcal{I}}_\infty$ decreases in magnitude as λ is increased for all values of p.

Turning our attention to the system dynamics using (8), the disorder-averaged evolution $\overline{\mathcal{I}}_t$ develops a bump as λ is increased from 0, as shown in Fig. 6(b), indicative of short-time correlations induced by the weakly entangling coherent hopping, before being destroyed by dissipation. The parametric dependence of this bump is shown in Appendix G.

IX. CONCLUSIONS

We explored the phenomena of entanglement phase transitions and heterogeneity in the stationary states of open quantum systems, using quadratic fermionic Lindbladians as a test bed. We observed a phase transition from area to volume law entanglement phases in a model with disordered, long-range bath interactions as a function of the range of interactions.

This correlates with a transition from nonlocal to local bath-system interactions, detected through the spread of individual jump operators. In the volume-law phase, the steady-state occupation is homogeneous, while the area-law phase exhibits significant heterogeneity which survives in the thermodynamic limit. Finally, perturbing with coherent hopping leaves the critical point unchanged, but induces increased short-time correlations.

Our work analyzed entanglement in mixed steady states of open quantum systems and shows the significance of disordered, long-range bath interactions in the entanglement scaling laws of dissipative systems. The persistence of entanglement in the presence of dissipation can be potentially leveraged to stabilize novel correlated states away from thermal equilibrium. Stability of the phase transition in the presence of interactions could have relevance to aspects of many-body localization [110–115]. Furthermore, it would be illuminating to understand the consequences of this phenomenon to the closely related measurement-induced transitions of quantum trajectories [116,117].

ACKNOWLEDGMENTS

We would like to thank Christopher Turner, Dawid Paszko, and Marcin Szyniszewski for their valuable insights and discussions. A.P. and D.C.R. are funded by the European Research Council (ERC) under the EU's Horizon 2020 research and innovation program via Grant Agreement No. 853368. The authors acknowledge the use of the UCL Myriad High Performance Computing Facility (Myriad@UCL), and associated support services, in the completion of this work.

APPENDIX A: FURTHER MODEL DETAILS AND DISCUSSION

Our model begins from a general quadratic fermionic Lindbladian without superconductive terms in the Hamiltonian:

$$\frac{d}{dt}\rho(t) = -i\left[\sum_{n,m} h_{nm} c_n^\dagger c_m, \rho(t)\right] + \sum_{jk}\Gamma_{jk}\left(c_k^\dagger \rho(t) c_j - \frac{1}{2}\{c_j c_k^\dagger, \rho(t)\}\right) + \sum_{jk} B_{jk}\left(c_j \rho(t) c_k^\dagger - \frac{1}{2}\{c_k^\dagger c_j, \rho(t)\}\right), \tag{A1}$$

from which a closed equation for the time evolution of the two-point correlation matrix $\Omega_{jk} = \mathrm{Tr}(\rho c_j^\dagger c_k)$ can be derived by multiplying (A1) by $c_j^\dagger c_k$ and then taking the trace [55]; after some algebra we obtain

$$\frac{d}{dt}\Omega(t) = i[h^T, \Omega(t)] + \frac{1}{2}\{\Gamma, \mathbb{I} - \Omega(t)\} - \frac{1}{2}\{B, \Omega\}. \tag{A2}$$

This equation is guaranteed to keep the correlation matrix physical due to constraints inherited from the Lindblad equation: Hermiticity is ensured by the Hermiticity of Γ, B, and h; positivity is ensured by the positivity of Γ and B. Physically, Γ and B correspond to competing bath interactions which respectively add and remove particles from the system. Existing in isolation, Γ would push the system into a state where every site is occupied by a particle, while B would lead to only holes.

We specifically focus on the case when $[\Gamma, B] = 0$. The eigenvalues $\{\alpha_n\}$ of Γ and $\{\beta_n\}$ of B and their corresponding eigenvectors $\{|g_n\rangle\}$ fully describe the behavior of the dissipation. In the case when $h = 0$, the eigenstates may be thought of as describing quasiparticle modes of the system: in the Lindbladian description, these eigenstates may be used to diagonalize the dissipative term, with each state resulting in a potentially delocalized jump operator $d_m = \sum_i \langle i|g_m\rangle c_i$.

Since we assume Γ and B commute, these jump operators appear in conjugate pairs which add and remove excitations from these modes at rates determined by the corresponding eigenvalues. The likelihood of these modes being occupied is therefore described by the ratios $\alpha^n/\beta^n \in (0, \infty)$, which may be thought of as representing the relationship between the energy of each mode and the temperature of the bath it is coupled to.

Finally, we further specialize to the case when $B = \mathbb{I} - \Gamma$, simplifying Eq. (A2) to

$$\frac{d}{dt}\Omega(t) = i[h^T, \Omega(t)] + \Gamma - \Omega(t). \tag{A3}$$

In the spectral basis of h the equations for each component decouple,

$$\frac{d}{dt}\widetilde{\Omega(t)}_{nm} = i(E_n - E_m + i)\widetilde{\Omega(t)}_{nm} + \widetilde{\Gamma}_{nm}, \tag{A4}$$

where E_n are the eigenvalues of h and $\widetilde{O}_{nm}$ denotes the matrix elements of O in h's basis. The solution to Eq. (A3) is then

$$\widetilde{\Omega(t)}_{nm} = e^{-t}\left(\widetilde{\Omega(0)}_{nm} - \frac{i\widetilde{\Gamma}_{nm}}{\Delta E_{nm}}\right)e^{i(E_n - E_m)t} + \frac{i\widetilde{\Gamma}_{nm}}{\Delta E_{nm}}, \tag{A5}$$

where $\Delta E_{nm} \doteq E_n - E_m + i$. Note that the steady state is independent of the initial conditions, indicating it is unique. A key benefit of the above is that it is numerically efficient to construct its time evolution and its stationary state up to and beyond a system size of 10^4 sites.

In the absence of H, Eq. (A5) reads

$$\Omega_{nm}(t) = \Gamma_{nm}(1 - e^{-t}) + \Omega_{nm}(0)e^{-t}, \tag{A6}$$

in the original basis of Γ.

APPENDIX B: EXACT SOLUTION WITHOUT HAMILTONIAN TERM

In the case when $h = 0$, an exact solution can be accessed by first separating the system into a set of independent fermionic modes based on the spectrum of Γ, then solving each independent system, as follows. For generality we show the result here for when $[\Gamma, B] = 0$, rather than any specific B which satisfies this equation. Writing the spectrum of Γ as $\Gamma\,|g_i\rangle = \gamma_i\,|g_i\rangle$, and the eigenvalues of B as b_i, we may rewrite our Lindbladian as

$$\begin{aligned}\mathcal{L}(\rho) &= \sum_m \left[\gamma_m d_m^\dagger \rho d_m - \frac{\gamma_m}{2}\{\rho, d_m d_m^\dagger\} b_m d_m^\dagger \rho d_m \right.\\ &\quad \left. - \frac{b_m}{2}\{\rho, d_m d_m^\dagger\}\right]\\ &= \sum_m \mathcal{L}_m(\rho),\end{aligned} \tag{B1}$$

where $d_m = \sum_i \langle i|g_m\rangle c_i$. Each term in this sum corresponds to an independent 2-level fermionic mode evolving according to a 4×4 Lindbladian.

For a given independent subsystem, with basis $|0_m\rangle$, $|1_m\rangle$ such that $d_m^\dagger\,|0_m\rangle = |1_m\rangle$ and $d_m\,|1_m\rangle = |0_m\rangle$, we calculate the matrix elements $\mathrm{Tr}[|i_m\rangle\,\langle j_m|\,\mathcal{L}_m(|i'_m\rangle\,\langle j'_m|)]$. Ordering the basis as $|1_m\rangle\,\langle 1_m|$, $|0_m\rangle\,\langle 0_m|$, $|0_m\rangle\,\langle 1_m|$, $|1_m\rangle\,\langle 0_m|$ we find

$$\mathcal{L}_m = \begin{pmatrix} -b_m & \gamma_m & 0 & 0 \\ b_m & -\gamma_m & 0 & 0 \\ 0 & 0 & -\frac{\gamma_m + b_m}{2} & 0 \\ 0 & 0 & 0 & -\frac{\gamma_m + b_m}{2} \end{pmatrix}, \tag{B2}$$

finding that the coherences are already eigenmodes, while the occupation expectations support a 2×2 block. This may be diagonalized to find eigenvalues of 0 and $-\gamma_m - b_m$, with corresponding left and right eigenvectors. Eigenmodes of the full Lindbladian can then be constructed by taking tensor products of the eigenmodes of each independent fermionic mode, and rewriting the state in terms of the original position-space creation and annihilation operators, with their corresponding eigenvalues given by the sum of the eigenvalues for each subsystem eigenmode used in the product.

In the case where $b_m = 1 - \gamma_m$, as we have in the main text, this result explains why our correlation matrix evolution equation has a uniform relaxation rate of 1, independent of system size and p. Since in this case the eigenvalues of each single-fermion Lindbladian are either 0, $-1/2$, or -1, eigenvalues of the full Lindbladian must be multiples of $-1/2$. Considering the space of quadratic states, there are three classes of terms which contribute: $d_m^\dagger d_m = |1_m\rangle\,\langle 1_m|$, $d_m d_m^\dagger = |0_m\rangle\,\langle 0_m|$, $d_m^\dagger d_n = |1_m\rangle\,\langle 0_m| \otimes |0_n\rangle\,\langle 1_n|$. The first two have support only on single-fermion eigenmodes with eigenvalues of 0 and -1, while the third consists of a tensor product of two single-fermion eigenmodes each with eigenvalue $-1/2$, and thus has an overall eigenvalues of -1. As such, all quadratic states reside in a vector subspace with support on eigenmodes with eigenvalues of 0 and -1. Since Gaussian states are a subspace of such matrices, they reside in the same vector subspace, and therefore possess the same uniform relaxation time of 1, also imparted on the evolution of their correlation matrices. We therefore see that this relaxation time, and its parameter independence, has its origin in the precise relationship we chose in taking $B = I - \Gamma$, leading to a particular balancing of transition rates in the classical stochastic evolution each independent fermionic mode undergoes.

APPENDIX C: MULTIFRACTALITY

To further understand the intermediate region between phases, particularly notable in the participation ratio, we calculate the generalized fractal dimensions encoding the scaling behavior of moments, as considered in other works on PRBMs [107,108]. For a given eigenstate ψ viewed as a single-particle wave function in a 1D system with L sites, we denote the probability of the particle being found in a box from i to $i + l - 1$ as

$$p_l(i) = \sum_{j=i}^{i+l-1} |\psi_j|^2. \tag{C1}$$

The qth moment of this probability distribution over disjoint boxes of length l is given by

$$\chi_q(l, L) = \sum_{i=0}^{L/l} p_l^q(il). \tag{C2}$$

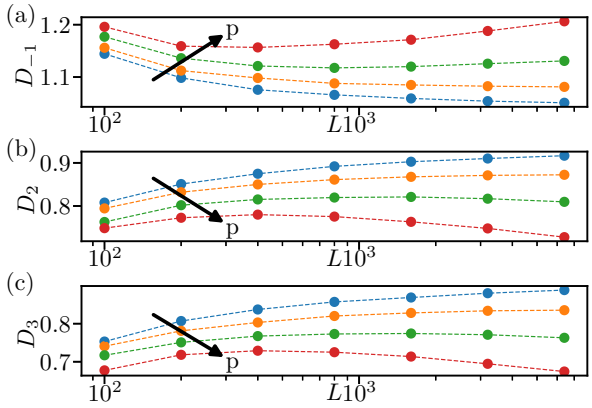

FIG. 7. (a)–(c) Generalized fractal dimensions as a function of system size for $p = [0.95, 1.0, 1.05, 1.1]$, increasing along the arrow.

Finally, the generalized fractal dimensions are then extracted from the scaling behavior of these moments. Assuming the moments satisfy a large deviation principle

$$\chi_q(l, L) \propto \left(\frac{l}{L}\right)^{D_q}, \tag{C3}$$

we have

$$D_q = \lim_{\delta \to 0} \frac{\ln[\chi_q(\delta L, L)]}{\ln(\delta)}, \tag{C4}$$

where $\delta = l/L$ is the fraction of the system contained in each region. Figure 7 shows how estimates of these change as L increase for a variety of q and p. We note two properties of this data consistent with multifractal phenomena [107–109]. First, in the vicinity of $p = 1.0$ the dimensions become approximately constant at large L, diverging away from this constant with L for p further from the critical point. When these exponents become independent of system size for all moments, the statistical properties of the particle's position depend only on the size of the subsystem relative to the total system size, not the absolute subsystem size. Second, the fractal dimension attains noticeably distinct values as q is varied, in contrast to non- and mono-fractal systems in which the fractal dimension remains largely constant.

APPENDIX D: $\overline{\text{PR}}$ FIT

In the main text, the fitting function $\overline{\text{PR}}(L, p) = L^{a(p)}/c(p)$ used to study the scaling behavior of the $\overline{\text{PR}}$ contains two parameters: the exponent a mentioned in the main text, and an overall scaling coefficient c. For completeness, in Fig. 8(a) we show the p dependence for both these coefficients. For comparison, in Fig. 8(b) we also show the exponent $a(p)$ found when fitting $c(p) = 1$ for all p: the lack of $c(p)$ to allow scaling to increase the overall $\overline{\text{PR}}$ produced by the fit, a key to accurately fitting in the intermediate regime, results in a slower decay of the exponent as p is increased. However, the overall behavior is qualitatively the same.

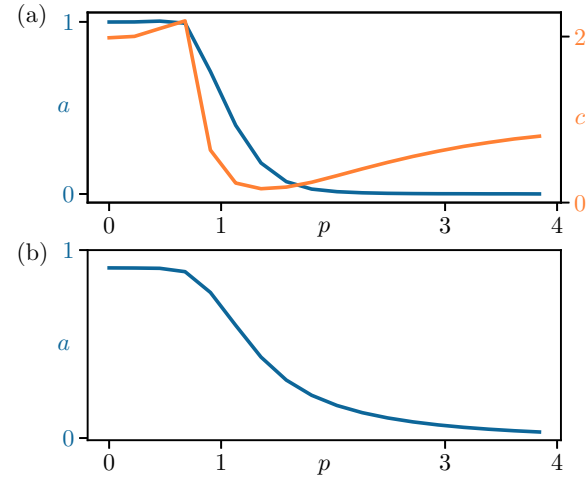

FIG. 8. Coefficients as a function of p found when fitting $\overline{\text{PR}}(L, p) = L^{a(p)}/c(p)$ to $\overline{\text{PR}}(L)$ curves.

APPENDIX E: NUMERICAL PROPERTIES OF Γ

1. Maximum eigenvalue statistics

The behavior of the largest eigenvalue of $X^\dagger X$, $\lambda_{\max}$, is of great importance to the dynamical study of ρ because

$$\Gamma \doteq X^\dagger X / 2\lambda_{\max}, \tag{E1}$$

as previously defined in the main text (which choice again tamed the semipositiveness of ρ). This maps the spectrum of Γ to the [0,1] interval regardless of p or L. Thus, it is worth studying the behavior of $\lambda_{\max}$ used for this definition of Γ for different values of p and L, Fig. 9. One finds that in the localized phase $\lambda_{\max}$ remains roughly fixed at a constant value for all such p and L whereas in the thermal phase $\lambda_{\max}$ grows as a power law with L.

2. Power-law decay of Γ matrix elements

Γ's matrix elements decay away from the diagonal as the distance to it, d, is increased. This decay is intimately related to p via

$$X_{jk} = \frac{x_{jk}}{(|j-k|+1)^p}. \tag{E2}$$

As depicted in Fig. 10, for large enough d, the decay of the matrix elements of Γ away from the diagonal is roughly given

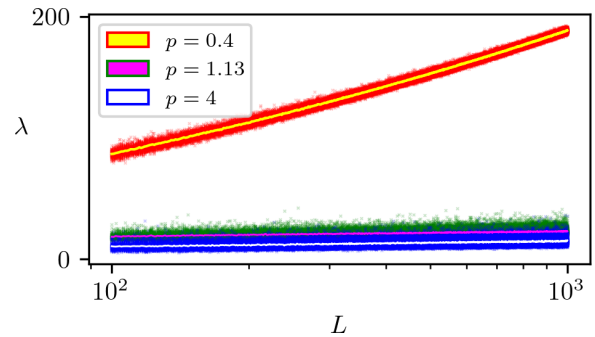

FIG. 9. Eigenvalues of $X^\dagger X$ (markers) and their average against L (lines).

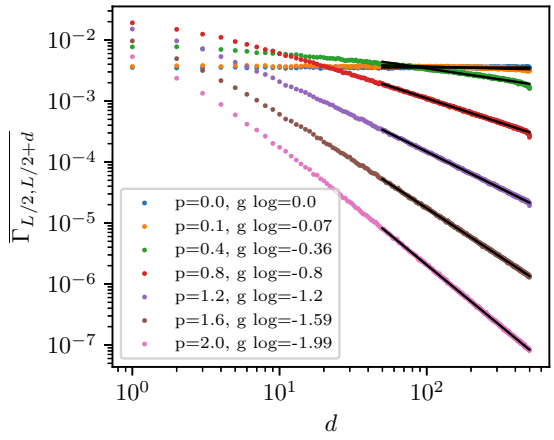

FIG. 10. Log-log plot of the decay of the matrix elements of Γ as a distance d away from the diagonal. For large enough d, the decay is given by a power law with an exponent approximately equal to p. In the legend, g log is the linear gradient of the black lines fitted to the log-log data. Note how $p \sim g\log$, suggesting a power-law decay with power p for large enough d.

by

$$||\Gamma_{L/2,L/2+d}|| \sim \frac{1}{d^p} \quad \text{for} \quad 1 \ll d. \tag{E3}$$

As Γ is Hermitian, this observation connects the localization transition of Γ's eigenvectors to the already mentioned power-banded localized Hamiltonian models in the literature.

3. Power-law decay of Γ eigenvectors

Prior studies of PRBMs have observed power-law decay of eigenstates away from a central site, particularly closer to the transition within the localized phase. This is in contrast to eigenstates in short-range models exhibiting exponential decay. In Fig. 11 we present data suggesting our PRBM model exhibits the same phenomena, with small deviations from power-law behavior at lower values of p.

APPENDIX F: MUTUAL INFORMATION WITH BOUNDARIES

When we set to explore the mutual information behavior between two subsystems, one needs to choose whether or not to include the boundaries that separate these two subsystems. In the main text, we decided to exclude the boundaries between A and B so when $L \to \infty$ even if A/L and B/L are set constant the boundary ∂_{AB} contribution to $\overline{\mathcal{I}}_\infty$ dies off as ∂_{AB} grows. This is because it filters the very short-range entanglement contribution of ∂_{AB} for sufficiently large L. This can be seen in the area-law phase in Fig. 1 of the main text. Here we redo our analysis of the mutual information without removing ∂_{AB} in Fig. 12. As expected, p_c shifts into the area-law phase as now the short-range entanglement is a more dominant contribution to $\overline{\mathcal{I}}_\infty$. This also illustrates the strength of this contribution toward $\overline{\mathcal{I}}_\infty$, which can be seen in this shift and the overall substantially larger magnitude of $\overline{\mathcal{I}}_\infty$. Note that in contrast to the unusual L_A dependence we observe in the case without boundary

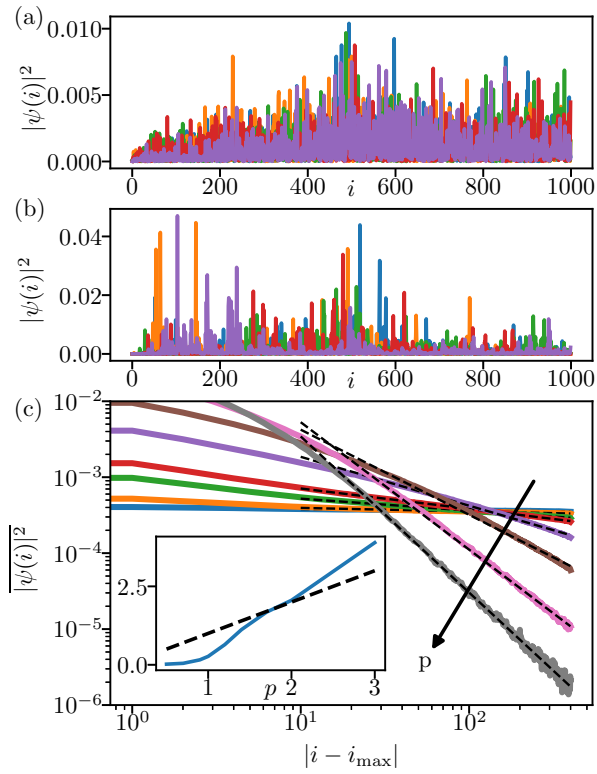

FIG. 11. (a), (b) Five sample eigenstates with a maximum magnitude value within the middle 25th of the system at (a) $p = 0.5$ and (b) $p = 1.1$. (c) Log-log plot of the averaged positional probability as a function of distance from the most probable site, for $p = [0.5, 0.7, 0.9, 1.0, 1.2, 1.4, 1.7, 2.0]$. Averaged over eigenstates with most probable sites located in the middle 5th of the system, and averaged over 1000 disorder realizations. Linear fits of the probabilities for distances of 100 to 1000 are shown by the dashed lines. Inset: (solid) gradients of the linear fits are shown vs p, (dashed) the curve $y = p$.

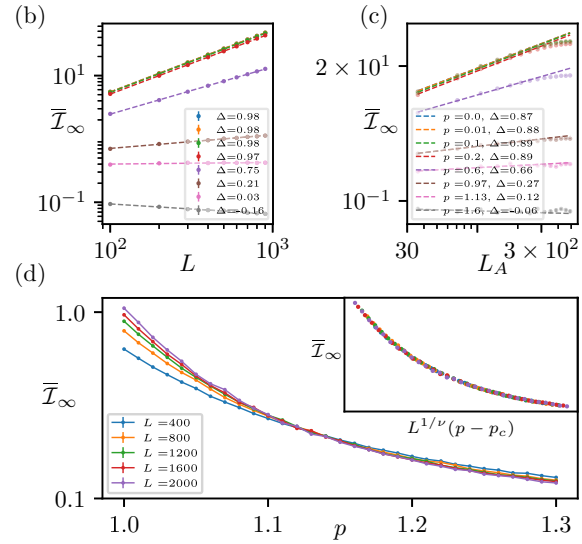

FIG. 12. Steady-state mutual information between A and B including their boundary term ∂_{AB}.

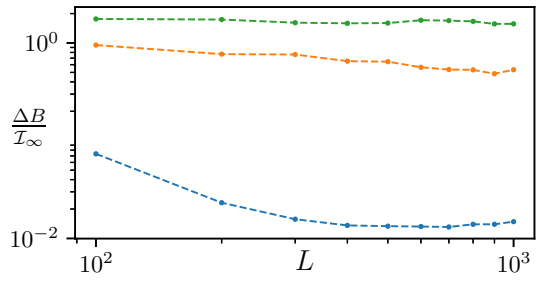

FIG. 13. Relative height of the bump in $\overline{\mathcal{I}}_t$ in (b) with respect to its $\overline{\mathcal{I}}_\infty$ scaled by $1/\overline{\mathcal{I}}_\infty$, denoted by $\Delta B/\overline{\mathcal{I}}_\infty$, against system size, L.

contributions, here we see a clear change from a subextensive power-law dependence at low p to an area-law dependence at high p.

APPENDIX G: MUTUAL INFORMATION BUMP

The height of the bump, ΔB, relative to $\overline{\mathcal{I}}_\infty$ at different values of p against L is plotted in Fig. 13. As L is increased, $\Delta B/\overline{\mathcal{I}}_\infty$ decreases for all p, but far more rapidly in the delocalized phase. The weak entangling nature of hopping introduces a short time increment in $\overline{\mathcal{I}}_t$ which is subsequently destroyed by the dissipation.

APPENDIX H: NUMERICAL DETAILS

1. Disorder realizations

In Fig. 1 of the main text, panel (b), disorder realizations are linearly decreased from 500 at $L = 100$ to 100 at $L = 1000$. In panel (c), 20 disorder realizations were used. Figure 2 of the main text uses identical disorder realizations to Fig. 1. In Fig. 3 of the main text, from $L = 400$ to $L = 2000$, disorder realizations were [500,200,200,200,100]. The inset of Fig. 3 of the main text was done using identical numbers of disorder realizations.

Figure 5 of the main text was computed by randomly generating Γ at each p, 10^3 times, and from this obtaining the temperature distribution shown. The inset was computed at $L = [50, 100, \ldots, 1000]$ and averaged with disorder realizations $[2000, 1900, \ldots, 100]$, respectively, for each value of p.

Figure 9 was computed by randomly sampling $X^\dagger X$ in the $L = [10^2, 10^3]$ interval 10^5 times for each value of p shown.

Figure 10 was computed at $L = 10^3$ and averaged over 10^3 realizations.

2. Finite-size scaling

To perform a finite-size scaling analysis on the mutual information data, we optimize a standard loss function which measures the spread of the data; see, e.g., Ref. [118]. Given that our data possess nonzero error bars from averaging over disorder realizations, we perform this analysis by sampling Gaussian perturbations of our dataset, sampling noise for each data point with a standard deviation equal to the error in the mean for that data point. For each sample of a noise-perturbed dataset, we then optimize the loss to find a corresponding critical point and exponent. The expected value and variance of these resulting parameters are then calculated, using 1000 noisy realizations of our dataset.

[1] H. P. Breuer and F. Petruccione, *The Theory of Open Quantum Systems* (Oxford University Press, Oxford, 2002).

[2] W. H. Zurek, Decoherence, einselection, and the quantum origins of the classical, Rev. Mod. Phys. **75**, 715 (2003).

[3] W. Dür and H.-J. Briegel, Stability of macroscopic entanglement under decoherence, Phys. Rev. Lett. **92**, 180403 (2004).

[4] M. Schlosshauer, Decoherence, the measurement problem, and interpretations of quantum mechanics, Rev. Mod. Phys. **76**, 1267 (2005).

[5] J. T. Barreiro, P. Schindler, O. Gühne, T. Monz, M. Chwalla, C. F. Roos, M. Hennrich, and R. Blatt, Experimental multiparticle entanglement dynamics induced by decoherence, Nat. Phys. **6**, 943 (2010).

[6] F. Reiter, A. S. Sørensen, P. Zoller, and C. Muschik, Dissipative quantum error correction and application to quantum sensing with trapped ions, Nat. Commun. **8**, 1822 (2017).

[7] P. M. Harrington, E. J. Mueller, and K. W. Murch, Engineered dissipation for quantum information science, Nat. Rev. Phys. **4**, 660 (2022).

[8] T. Ilias, D. Yang, S. F. Huelga, and M. B. Plenio, Criticality-enhanced quantum sensing via continuous measurement, PRX Quantum **3**, 010354 (2022).

[9] M. Žnidarič, T. Prosen, G. Benenti, G. Casati, and D. Rossini, Thermalization and ergodicity in one-dimensional many-body open quantum systems, Phys. Rev. E **81**, 051135 (2010).

[10] I. Reichental, A. Klempner, Y. Kafri, and D. Podolsky, Thermalization in open quantum systems, Phys. Rev. B **97**, 134301 (2018).

[11] F. Verstraete, M. M. Wolf, and J. I. Cirac, Quantum computation and quantum-state engineering driven by dissipation, Nat. Phys. **5**, 633 (2009).

[12] S. Diehl, E. Rico, M. A. Baranov, and P. Zoller, Topology by dissipation in atomic quantum wires, Nat. Phys. **7**, 971 (2011).

[13] C.-E. Bardyn, M. A. Baranov, C. V. Kraus, E. Rico, A. İmamoğlu, P. Zoller, and S. Diehl, Topology by dissipation, New J. Phys. **15**, 085001 (2013).

[14] M. Žnidarič, Relaxation times of dissipative many-body quantum systems, Phys. Rev. E **92**, 042143 (2015).

[15] D. Paszko, D. C. Rose, M. H. Szymańska, and A. Pal, Edge modes and symmetry-protected topological states in open quantum systems, arXiv:2310.09406.

[16] P. Zanardi, Dissipative dynamics in a quantum register, Phys. Rev. A **56**, 4445 (1997).

[17] P. Zanardi and M. Rasetti, Noiseless quantum codes, Phys. Rev. Lett. **79**, 3306 (1997).

[18] D. A. Lidar, I. L. Chuang, and K. B. Whaley, Decoherence-free subspaces for quantum computation, Phys. Rev. Lett. **81**, 2594 (1998).

[19] E. Knill, R. Laflamme, and L. Viola, Theory of quantum error correction for general noise, Phys. Rev. Lett. **84**, 2525 (2000).

[20] P. Zanardi, Stabilizing quantum information, Phys. Rev. A **63**, 012301 (2000).
[21] V. V. Albert, B. Bradlyn, M. Fraas, and L. Jiang, Geometry and response of Lindbladians, Phys. Rev. X **6**, 041031 (2016).
[22] G. T. Landi, D. Poletti, and G. Schaller, Non-equilibrium boundary driven quantum systems: Models, methods and properties, Rev. Mod. Phys. **94**, 045006 (2022).
[23] L. M. Sieberer, M. Buchhold, and S. Diehl, Keldysh field theory for driven open quantum systems, Rep. Prog. Phys. **79**, 096001 (2016).
[24] M. F. Maghrebi and A. V. Gorshkov, Nonequilibrium many-body steady states via Keldysh formalism, Phys. Rev. B **93**, 014307 (2016).
[25] E. G. Dalla Torre, S. Diehl, M. D. Lukin, S. Sachdev, and P. Strack, Keldysh approach for nonequilibrium phase transitions in quantum optics: Beyond the Dicke model in optical cavities, Phys. Rev. A **87**, 023831 (2013).
[26] K. Macieszczak, M. Guţă, I. Lesanovsky, and J. P. Garrahan, Towards a theory of metastability in open quantum dynamics, Phys. Rev. Lett. **116**, 240404 (2016).
[27] D. C. Rose, K. Macieszczak, I. Lesanovsky, and J. P. Garrahan, Metastability in an open quantum Ising model, Phys. Rev. E **94**, 052132 (2016).
[28] K. Macieszczak, D. C. Rose, I. Lesanovsky, and J. P. Garrahan, Theory of classical metastability in open quantum systems, Phys. Rev. Res. **3**, 033047 (2021).
[29] D. C. Rose, K. Macieszczak, I. Lesanovsky, and J. P. Garrahan, Hierarchical classical metastability in an open quantum East model, Phys. Rev. E **105**, 044121 (2022).
[30] F. Iemini, A. Russomanno, J. Keeling, M. Schirò, M. Dalmonte, and R. Fazio, Boundary time crystals, Phys. Rev. Lett. **121**, 035301 (2018).
[31] B. Zhu, J. Marino, N. Y. Yao, M. D. Lukin, and E. A. Demler, Dicke time crystals in driven-dissipative quantum many-body systems, New J. Phys. **21**, 073028 (2019).
[32] F. M. Gambetta, F. Carollo, M. Marcuzzi, J. P. Garrahan, and I. Lesanovsky, Discrete time crystals in the absence of manifest symmetries or disorder in open quantum systems, Phys. Rev. Lett. **122**, 015701 (2019).
[33] A. Riera-Campeny, M. Moreno-Cardoner, and A. Sanpera, Time crystallinity in open quantum systems, Quantum **4**, 270 (2020).
[34] J. O'Sullivan, O. Lunt, C. W. Zollitsch, M. L. W. Thewalt, J. J. L. Morton, and A. Pal, Signatures of discrete time crystalline order in dissipative spin ensembles, New J. Phys. **22**, 085001 (2020).
[35] H. Keßler, P. Kongkhambut, C. Georges, L. Mathey, J. G. Cosme, and A. Hemmerich, Observation of a dissipative time crystal, Phys. Rev. Lett. **127**, 043602 (2021).
[36] G. Passarelli, P. Lucignano, R. Fazio, and A. Russomanno, Dissipative time crystals with long-range Lindbladians, Phys. Rev. B **106**, 224308 (2022).
[37] B. Buča, J. Tindall, and D. Jaksch, Non-stationary coherent quantum many-body dynamics through dissipation, Nat. Commun. **10**, 1730 (2019).
[38] J. P. Garrahan and I. Lesanovsky, Thermodynamics of quantum jump trajectories, Phys. Rev. Lett. **104**, 160601 (2010).
[39] F. Carollo, J. P. Garrahan, I. Lesanovsky, and C. Pérez-Espigares, Making rare events typical in Markovian open quantum systems, Phys. Rev. A **98**, 010103(R) (2018).
[40] F. Carollo, R. L. Jack, and J. P. Garrahan, Unraveling the large deviation statistics of Markovian open quantum systems, Phys. Rev. Lett. **122**, 130605 (2019).
[41] F. Carollo and C. Pérez-Espigares, Entanglement statistics in Markovian open quantum systems: A matter of mutation and selection, Phys. Rev. E **102**, 030104(R) (2020).
[42] F. Carollo, J. P. Garrahan, and R. L. Jack, Large deviations at level 2.5 for Markovian open quantum systems: Quantum jumps and quantum state diffusion, J. Stat. Phys. **184**, 13 (2021).
[43] B. Olmos, I. Lesanovsky, and J. P. Garrahan, Facilitated spin models of dissipative quantum glasses, Phys. Rev. Lett. **109**, 020403 (2012).
[44] B. Olmos, I. Lesanovsky, and J. P. Garrahan, Out-of-equilibrium evolution of kinetically constrained many-body quantum systems under purely dissipative dynamics, Phys. Rev. E **90**, 042147 (2014).
[45] I. Lesanovsky, M. van Horssen, M. Guţă, and J. P. Garrahan, Characterization of dynamical phase transitions in quantum jump trajectories beyond the properties of the stationary state, Phys. Rev. Lett. **110**, 150401 (2013).
[46] S. Marcantoni, C. Pérez-Espigares, and J. P. Garrahan, Symmetry-induced fluctuation relations in open quantum systems, Phys. Rev. E **104**, 014108 (2021).
[47] J. M. Hickey, S. Genway, I. Lesanovsky, and J. P. Garrahan, Thermodynamics of quadrature trajectories in open quantum systems, Phys. Rev. A **86**, 063824 (2012).
[48] Y. Li, X. Chen, and M. P. A. Fisher, Measurement-driven entanglement transition in hybrid quantum circuits, Phys. Rev. B **100**, 134306 (2019).
[49] B. Skinner, J. Ruhman, and A. Nahum, Measurement-induced phase transitions in the dynamics of entanglement, Phys. Rev. X **9**, 031009 (2019).
[50] Y. Li, X. Chen, and M. P. A. Fisher, Quantum Zeno effect and the many-body entanglement transition, Phys. Rev. B **98**, 205136 (2018).
[51] T. Prosen, Third quantization: A general method to solve master equations for quadratic open Fermi systems, New J. Phys. **10**, 043026 (2008).
[52] T. Prosen and I. Pižorn, Quantum phase transition in a far-from-equilibrium steady state of an XY spin chain, Phys. Rev. Lett. **101**, 105701 (2008).
[53] C. Guo and D. Poletti, Solutions for bosonic and fermionic dissipative quadratic open systems, Phys. Rev. A **95**, 052107 (2017).
[54] T. Prosen, Spectral theorem for the Lindblad equation for quadratic open fermionic systems, J. Stat. Mech.: Theory Exp. (2010) P07020.
[55] R. Mahajan, C. D. Freeman, S. Mumford, N. Tubman, and B. Swingle, Entanglement structure of non-equilibrium steady states, arXiv:1608.05074.
[56] C. Zanoci and B. Swingle, Entanglement and thermalization in open fermion systems, arXiv:1612.04840.
[57] S. Lieu, M. McGinley, and N. R. Cooper, Tenfold way for quadratic Lindbladians, Phys. Rev. Lett. **124**, 040401 (2020).
[58] T. Barthel and Y. Zhang, Solving quasi-free and quadratic Lindblad master equations for open fermionic and bosonic systems, J. Stat. Mech.: Theory Exp. (2022) 113101.

[59] A. D'Abbruzzo, V. Alba, and D. Rossini, Logarithmic entanglement scaling in dissipative free-fermion systems, Phys. Rev. B **106**, 235149 (2022).

[60] J. Costa, P. Ribeiro, A. de Luca, T. Prosen, and L. Sá, Spectral and steady-state properties of fermionic random quadratic Liouvillians, SciPost Phys. **15**, 145 (2023).

[61] E. Vernier, Mixing times and cutoffs in open quadratic fermionic systems, SciPost Phys. **9**, 049 (2020).

[62] S. Denisov, T. Laptyeva, W. Tarnowski, D. Chruściński, and K. Życzkowski, Universal spectra of random Lindblad operators, Phys. Rev. Lett. **123**, 140403 (2019).

[63] T. Can, V. Oganesyan, D. Orgad, and S. Gopalakrishnan, Spectral gaps and midgap states in random quantum master equations, Phys. Rev. Lett. **123**, 234103 (2019).

[64] T. Can, Random Lindblad dynamics, J. Phys. A: Math. Theor. **52**, 485302 (2019).

[65] L. Sá, P. Ribeiro, T. Can, and T. Prosen, Spectral transitions and universal steady states in random Kraus maps and circuits, Phys. Rev. B **102**, 134310 (2020).

[66] L. Sá, P. Ribeiro, and T. Prosen, Spectral and steady-state properties of random Liouvillians, J. Phys. A: Math. Theor. **53**, 305303 (2020).

[67] K. Wang, F. Piazza, and D. J. Luitz, Hierarchy of relaxation timescales in local random Liouvillians, Phys. Rev. Lett. **124**, 100604 (2020).

[68] O. E. Sommer, F. Piazza, and D. J. Luitz, Many-body hierarchy of dissipative timescales in a quantum computer, Phys. Rev. Res. **3**, 023190 (2021).

[69] W. Tarnowski, I. Yusipov, T. Laptyeva, S. Denisov, D. Chruściński, and K. Życzkowski, Random generators of Markovian evolution: A quantum-classical transition by superdecoherence, Phys. Rev. E **104**, 034118 (2021).

[70] S. Lange and C. Timm, Random-matrix theory for the Lindblad master equation, Chaos **31**, 023101 (2021).

[71] J. L. Li, D. C. Rose, J. P. Garrahan, and D. J. Luitz, Random matrix theory for quantum and classical metastability in local Liouvillians, Phys. Rev. B **105**, L180201 (2022).

[72] D. Orgad, V. Oganesyan, and S. Gopalakrishnan, Dynamical transitions from slow to fast relaxation in random open quantum systems, Phys. Rev. Lett. **132**, 040403 (2024).

[73] R. Yamamoto, J. Kobayashi, T. Kuno, K. Kato, and Y. Takahashi, An ytterbium quantum gas microscope with narrow-line laser cooling, New J. Phys. **18**, 023016 (2016).

[74] J. Marino, Universality class of Ising critical states with long-range losses, Phys. Rev. Lett. **129**, 050603 (2022).

[75] K. Seetharam, A. Lerose, R. Fazio, and J. Marino, Dynamical scaling of correlations generated by short- and long-range dissipation, Phys. Rev. B **105**, 184305 (2022).

[76] M. A. Norcia, A. W. Young, and A. M. Kaufman, Microscopic control and detection of ultracold strontium in optical-tweezer arrays, Phys. Rev. X **8**, 041054 (2018).

[77] M. Miranda, R. Inoue, N. Tambo, and M. Kozuma, Site-resolved imaging of a bosonic Mott insulator using ytterbium atoms, Phys. Rev. A **96**, 043626 (2017).

[78] J. A. Needham, I. Lesanovsky, and B. Olmos, Subradiance-protected excitation transport, New J. Phys. **21**, 073061 (2019).

[79] R. Jones, J. A. Needham, I. Lesanovsky, F. Intravaia, and B. Olmos, Modified dipole-dipole interaction and dissipation in an atomic ensemble near surfaces, Phys. Rev. A **97**, 053841 (2018).

[80] P. Wang and R. Fazio, Dissipative phase transitions in the fully connected Ising model with p-spin interaction, Phys. Rev. A **103**, 013306 (2021).

[81] Y. V. Fyodorov and A. D. Mirlin, Scaling properties of localization in random band matrices: A σ-model approach, Phys. Rev. Lett. **67**, 2405 (1991).

[82] A. D. Mirlin, Y. V. Fyodorov, F.-M. Dittes, J. Quezada, and T. H. Seligman, Transition from localized to extended eigenstates in the ensemble of power-law random banded matrices, Phys. Rev. E **54**, 3221 (1996).

[83] G. Casati, L. Molinari, and F. Izrailev, Scaling properties of band random matrices, Phys. Rev. Lett. **64**, 1851 (1990).

[84] G. Casati, B. V. Chirikov, I. Guarneri, and F. M. Izrailev, Band-random-matrix model for quantum localization in conservative systems, Phys. Rev. E **48**, R1613 (1993).

[85] J. Schenker, Eigenvector localization for random band matrices with power law band width, Commun. Math. Phys. **290**, 1065 (2009).

[86] P. Bourgade, Random band matrices, arXiv:1807.03031.

[87] I. Varga, Fluctuation of correlation dimension and inverse participation number at the Anderson transition, Phys. Rev. B **66**, 094201 (2002).

[88] X. Cao, A. Rosso, J.-P. Bouchaud, and P. Le Doussal, Genuine localization transition in a long-range hopping model, Phys. Rev. E **95**, 062118 (2017).

[89] J. M. Magán, Random free fermions: An analytical example of eigenstate thermalization, Phys. Rev. Lett. **116**, 030401 (2016).

[90] T. Tao and V. Vu, Random matrices: Universal properties of eigenvectors, Random Matrices: Theory Appl. **01**, 1150001 (2012).

[91] I. Peschel and V. Eisler, Reduced density matrices and entanglement entropy in free lattice models, J. Phys. A: Math. Theor. **42**, 504003 (2009).

[92] J. Surace and L. Tagliacozzo, Fermionic Gaussian states: An introduction to numerical approaches, SciPost Phys. Lect. Notes 54, (2022).

[93] X. Jia, A. R. Subramaniam, I. A. Gruzberg, and S. Chakravarty, Entanglement entropy and multifractality at localization transitions, Phys. Rev. B **77**, 014208 (2008).

[94] P. Łydżba, M. Rigol, and L. Vidmar, Eigenstate entanglement entropy in random quadratic Hamiltonians, Phys. Rev. Lett. **125**, 180604 (2020).

[95] G. De Tomasi and I. M. Khaymovich, Multifractality meets entanglement: Relation for nonergodic extended states, Phys. Rev. Lett. **124**, 200602 (2020).

[96] M. Block, Y. Bao, S. Choi, E. Altman, and N. Y. Yao, Measurement-induced transition in long-range interacting quantum circuits, Phys. Rev. Lett. **128**, 010604 (2022).

[97] T. Minato, K. Sugimoto, T. Kuwahara, and K. Saito, Fate of measurement-induced phase transition in long-range interactions, Phys. Rev. Lett. **128**, 010603 (2022).

[98] T. Müller, S. Diehl, and M. Buchhold, Measurement-induced dark state phase transitions in long-ranged fermion systems, Phys. Rev. Lett. **128**, 010605 (2022).

[99] S. Sharma, X. Turkeshi, R. Fazio, and M. Dalmonte, Measurement-induced criticality in extended and long-range unitary circuits, SciPost Phys. Core **5**, 023 (2022).

[100] A. De Luca, B. L. Altshuler, V. E. Kravtsov, and A. Scardicchio, Anderson localization on the Bethe lattice: Nonergodicity of extended states, Phys. Rev. Lett. **113**, 046806 (2014).
[101] G. Parisi, S. Pascazio, F. Pietracaprina, V. Ros, and A. Scardicchio, Anderson transition on the Bethe lattice: An approach with real energies, J. Phys. A: Math. Theor. **53**, 014003 (2020).
[102] G. Vidal and R. F. Werner, Computable measure of entanglement, Phys. Rev. A **65**, 032314 (2002).
[103] R. Simon, Peres-Horodecki separability criterion for continuous variable systems, Phys. Rev. Lett. **84**, 2726 (2000).
[104] V. Eisler and Z. Zimborás, On the partial transpose of fermionic Gaussian states, New J. Phys. **17**, 053048 (2015).
[105] V. Alba and F. Carollo, Logarithmic negativity in out-of-equilibrium open free-fermion chains: An exactly solvable case, SciPost Phys. **15**, 124 (2023).
[106] C. Yeung and Y. Oono, A conjecture on nonlocal random tight-binding models, Europhys. Lett. **4**, 1061 (1987).
[107] E. Cuevas, V. Gasparian, and M. Ortuño, Anomalously large critical regions in power-law random matrix ensembles, Phys. Rev. Lett. **87**, 056601 (2001).
[108] E. Cuevas, Multifractality of Hamiltonians with power-law transfer terms, Phys. Rev. B **68**, 184206 (2003).
[109] N. Macé, F. Alet, and N. Laflorencie, Multifractal scalings across the many-body localization transition, Phys. Rev. Lett. **123**, 180601 (2019).
[110] E. Levi, M. Heyl, I. Lesanovsky, and J. P. Garrahan, Robustness of many-body localization in the presence of dissipation, Phys. Rev. Lett. **116**, 237203 (2016).
[111] M. V. Medvedyeva, T. Prosen, and M. Žnidarič, Influence of dephasing on many-body localization, Phys. Rev. B **93**, 094205 (2016).
[112] H. P. Lüschen, P. Bordia, S. S. Hodgman, M. Schreiber, S. Sarkar, A. J. Daley, M. H. Fischer, E. Altman, I. Bloch, and U. Schneider, Signatures of many-body localization in a controlled open quantum system, Phys. Rev. X **7**, 011034 (2017).
[113] Z. Lenarčič, E. Altman, and A. Rosch, Activating many-body localization in solids by driving with light, Phys. Rev. Lett. **121**, 267603 (2018).
[114] O. Lunt and A. Pal, Measurement-induced entanglement transitions in many-body localized systems, Phys. Rev. Res. **2**, 043072 (2020).
[115] J. Mák, M. Bhaseen, and A. Pal, Statics and dynamics of non-Hermitian many-body localization, Commun. Phys. **7**, 92 (2024).
[116] M. Szyniszewski, O. Lunt, and A. Pal, Disordered monitored free fermions, Phys. Rev. B **108**, 165126 (2023).
[117] P. Pöpperl, I. V. Gornyi, and Y. Gefen, Measurements on an Anderson chain, Phys. Rev. B **107**, 174203 (2023).
[118] A. Zabalo, M. J. Gullans, J. H. Wilson, S. Gopalakrishnan, D. A. Huse, and J. H. Pixley, Critical properties of the measurement-induced transition in random quantum circuits, Phys. Rev. B **101**, 060301(R) (2020).